FASDD: An Open-access 100,000-level Flame and Smoke Detection Dataset for Deep Learning in Fire Detection

Ming Wang[1], Liangcun Jiang[1, 2, 3] *, Peng Yue[1, 3, 4, 5]*, Dayu Yu[1], Tianyu Tuo[1]

[1] School of Remote Sensing and Information Engineering, Wuhan University, Wuhan, Hubei, 430079, China
5 [2] School of Resources and Environmental Engineering, Wuhan University of Technology, Wuhan, Hubei, 430070, China
[3] Hubei LuoJia Laboratory, Wuhan, Hubei, 430079, China
[4] Collaborative Innovation Center of Geospatial Technology, Wuhan, Hubei, 430079, China
[5] Hubei Province Engineering Center for Intelligent Geoprocessing (HPECIG), Wuhan University, Wuhan, Hubei, 430079, China
10 *Correspondence to*: Liangcun Jiang (jiangliangcun@whut.edu.cn); Peng Yue(pyue@whu.edu.cn)

Abstract. Deep learning methods driven by in situ video and remote sensing images have been used in fire detection. The performance and generalization of fire detection models, however, are restricted by the limited number and modality of fire detection training datasets. A large-scale fire detection benchmark dataset covering complex and varied fire scenarios is 15 urgently needed. This work constructs a 100,000-level Flame and Smoke Detection Dataset (FASDD) based on multi-source heterogeneous flame and smoke images. To the best of our knowledge, FASDD is currently the most versatile and comprehensive dataset for fire detection. It provides a challenging benchmark to drive the continuous evolution of fire detection models. Additionally, we formulate a unified workflow for preprocessing, annotation and quality control of fire samples. Meanwhile, out-of-the-box annotations are published in four different formats for training deep learning models. 20 Deep learning models trained on FASDD demonstrate the potential value and challenges of our dataset in fire detection and localization. Extensive performance evaluations based on classical methods show that most of the models trained on FASDD can achieve satisfactory fire detection results, and especially YOLOv5x achieves nearly 80% mAP@0.5 accuracy on heterogeneous images spanning two domains of computer vision and remote sensing. And the application in wildfire location demonstrates that deep learning models trained on our dataset can be used in recognizing and monitoring forest fires. 25 It can be deployed simultaneously on watchtowers, drones and optical satellites to build a satellite-ground cooperative observation network, which can provide an important reference for large-scale fire suppression, victim escape, firefighter rescue and government decision-making. The dataset is available from the Science Data Bank website at https://doi.org/10.57760/sciencedb.j00104.00103 (Wang et al., 2022).

1 Introduction

30 Fire is one of the most severe disasters that threaten human safety and Earth ecology (Gaur et al., 2020; Gibson et al., 2020; Shamsoshoara et al., 2021). Extreme forest fire accidents can cause severe economic losses and devastating ecological damage, lead to human respiratory and cardiovascular diseases, and even endanger human life (Chowdary et al., 2018; Gaur

et al., 2020). According to the 2022 report from International Association of Fire and Rescue Services, the frequency of global fire events has shown an increasing trend in the last decade (Brushlinsky et al., 2022). The seven-month-long Australian bushfire emergency in 2019, as a representative of extreme fire disasters, leaves a deep imprint on the Earth. Fire detection is a very crucial task in the pre-suppression process. However, the suddenness and scenario complexity of fire events bring tremendous challenges to the early detection and warning of fires. The development process of fire is generally manifested in two states: the initial wisps of light smoke and the subsequent raging fire. Fire detection methods that rely on traditional smoke sensors usually have low sensitivity or high false alarm rate (FAR). Smoke or heat takes a long time to diffuse, so it is difficult to achieve real-time alarm and timely stop loss (Gong et al., 2019; Bu et al., 2019). The vision-based fire detection methods have the advantages of low cost, rapid response, wide detection area, and remote visualization. However, in complex real-world environments, flame and smoke have multiple characteristics of flickering, growth, disorder, various colors, and variable intensity (Muhammad et al., 2018). Flame is also easily confused with many objects such as lights, sun and maple leaves, and smoke are easily confused with clouds, waterfalls and hair (Geetha et al., 2021). When coupled with the low signal-to-noise ratio scene, it brings additional difficulties to vision-based fire detection methods (Muhammad et al., 2018).

Vision-based fire detection methods mainly include static feature-based, dynamic feature-based, traditional machine learning-based, and neural network-based methods. Static feature-based methods usually implement fire discrimination based on representative features of flame and smoke such as color features (Foggia et al. 2015; Calderara et al. 2008). These static feature-based methods have lower computational costs, yet they also bring lower reliability and higher false alarm rates (Muhammad et al., 2018). Dynamic feature-based methods analyze flame and smoke videos based on flicker (Töreyin et al. 2005), motion and dynamic texture or the evolution of spatio-temporal information (Dimitropoulos et al. 2015). These methods employ the irregularity and growth properties of flame and smoke, which can improve the detection accuracy to some extent, yet it requires high computational cost. Traditional machine learning based methods perform fire detection with classical classifiers such as decision tree, support vector machines and random forest, which are usually trained based on hand crafted features (Chi et al. 2017; Wang et al. 2017). However, these methods face the feature selection bias problem and usually have a high operational complexity and time cost. In this context, neural network-based fire detection methods are emerging. Dua et al. (2020) detect fires based on deep convolutional neural networks (DCNN) and the Transfer Learning approach, which outperforms traditional machine learning models. Cheng et al. (2019) use the generative adversarial network (GAN) to predict the changing trend of smoke and improve the smoke segmentation accuracy based on Deeplabv3+ and DenseCRF.

Neural network-based methods have gradually developed into the mainstream fire detection methods, which can generally achieve satisfactory detection accuracy. Considering that visual features of flame and smoke have significant differences in different scenes, robust deep learning models usually require large-scale, high-quality training samples to drive (Torralba et al., 2011). Existing open-access training datasets for fire detection are oriented to specific modality data (such as visible light video, infrared thermal imaging video, and optical satellite imagery), specific tasks (such as image classification, object

detection, and semantic segmentation) or specific scenes (such as indoor fires and wildfires). Those datasets have some limitations such as small number of samples, fixed image size or resolution, single data source, poor task compatibility, and similar scenes. There is an urgent need to establish a training dataset with a large amount of heterogeneous flame and smoke

70   samples. Such a dataset shall be produced using a unified specification, and managed following FAIR (findability, accessibility, interoperability, and reusability) principles (Geetha et al., 2021).

In this paper, a large-scale heterogeneous Flame and Smoke Detection Dataset (FASDD) is provided, which includes fire data from multiple modalities and various scenarios. To overcome the limitations of existing datasets, we collected and carefully selected a large number of fire images captured by surveillance, drones, and multi-source remote sensing satellites,

75   which can provide data support for training robust fire detection models. The main contributions of this paper are briefly summarized as follows: (1) A 100,000-level flame and smoke detection dataset is constructed. To the best of our knowledge, it is the largest open-access fire dataset with the most complexity in fire scenes, the highest heterogeneity in image modality and feature distribution, and the most significant difference in image size and shape. It can support object detection and classification tasks in different fire scenes captured by various sensors. (2) The dataset is generated according to a unified

80   data model. Moreover, the annotation files are provided in four common dataset formats for FASDD to support different deep learning models. (3) Extensive performance comparison and evaluation based on representative object detection methods are performed on FASDD to provide a valuable reference for using our dataset.

2 Related work

2.1 Existing fire detection datasets

85   There are many works on datasets for fire detection. Jakovcevic et al. (2010) first propose a wildfire smoke dataset for the smoke segmentation task, which focuses on smoke in the wild. For the smoke classification task, Yuan (2011) provides a dataset that includes real-time smoke, synthetic smoke, non-smoke images, and videos. Chino et al. (2015) present a flame and smoke dataset that includes 240 training samples and 226 test samples. However, these datasets have a small sample size and are only applicable to simple classification tasks without accurate bounding box or mask labels. There are also some

90   datasets produced based on videos. Ko et al. (2012) publish a wildfire smoke video dataset. Foggia et al. (2015) provide an influential flame and smoke video dataset containing videos captured indoors and outdoors, during day and night, and at different distances. Zhang et al. (2018) introduce a wildfire smoke video dataset from watchtowers and UAVs (unmanned aerial vehicles). Shamsoshoara et al. (2021) describe a dataset for forest fire detection containing flame and smoke videos and aerial images captured by infrared cameras. Yet, there are many similar frames in these video datasets, and their

95   heterogeneity and generalizability are insufficient. Sharma et al. (2017) propose a flame image dataset containing flame images with different lighting intensities and scenes. Dunnings et al. (2018) from Durham University publish a flame dataset for the segmentation task, whose image size is set uniformly to 224 × 224 pixels. The image size in these datasets is relatively fixed and small, which cannot be easily generalized for other tasks or scenes. Geng et al. (2020) provide a large

dataset of flame and smoke for object detection tasks, but most of these images are unlabeled. These available flame and
100   smoke datasets have some limitations in terms of quantity, modality, resolution and scene (Geetha et al., 2021), but they
provide valuable references for developing a large-scale cross-domain fire detection dataset with different scenes and rich
characteristics.

2.2 Annotation tools

An appropriate data annotation tool is beneficial to optimize the data annotation process and improve the data annotation
105   efficiency (Geetha et al., 2021). Image annotation tools for object detection can be divided into offline tools and online tools
(Pande et al., 2022). Offline tools have high autonomy and controllability, which can ensure that data collection, cleaning,
labeling and training are implemented in a local network-free environment. LabelImg (Tzutalin, 2015) is widely used as
image annotation software for object detection. It supports PASCAL VOC (XML), YOLO (TXT) and CreateML annotation
formats and can be deployed on Windows, macOS and Linux operating systems. LabelMe (Wada et al., 2021) supports six
110   different bounding box shapes, including polygon, rectangle, circle, line, point, and line strip. One of its limitations is that
object labels can only be saved and exported in JSON format. GTCreator (Bernal et al., 2019) allows multiple annotators to
work simultaneously on the same task and offers full annotation editing and browsing capabilities. ByLabel (Qin et al., 2018)
is a boundary-based semiautomatic tool that simplifies labeling process by selecting among the boundary fragment proposals
that the tool automatically generates. However, offline tools may cause compatibility issues with the operating system.
115   Online tools allow data to be quickly annotated by enabling team collaboration. The VGG Image Annotator (VIA) tool
(Dutta and Zisserman, 2019) is an open source software that supports both offline and online annotation. Labels annotated in
VIA can be exported to plain text data formats like JSON and CSV. The downside of the tool is that it lacks dataset
management capabilities. ImageTagger (Fiedler et al., 2019) provides data and user management, manual and automatic
labeling, annotations validation, and collaboration capabilities. Its annotations can be exported to a user-defined format.
120   BRIMA (Lahtinen et al., 2021) creates a browser-based extension to help researchers and crowdsourcing contributors
conduct online image annotation. Its annotation files can only be exported to the JSON format of MS COCO. Labelbox
(Sharma et al., 2022) provides many advanced features such as collaboration, automation, data and user management, and
multiple format support. Yet, its basic version can only realize the labeling of rectangular boxes and polygons.

2.3 Training data specifications

125   Using a unified or common way to describe labels is essential to facilitate training data sharing (Geetha et al., 2021).
Common data formats for object detection tasks mainly include the JSON format adopted by the Microsoft COCO (Lin et al.,
2014) dataset, the XML format adopted by the PASCAL Visual Object Classes VOC (Everingham et al., 2015) dataset, and
the text format adopted by models of YOLO (Redmon et al., 2016) series. In COCO, a JSON annotation is created for
training, testing and validation on the entire dataset. The unique bounding box is represented by the coordinates of the upper
130   left corner, and the width and height of the bounding box. Its format can be described as [x, y, w, h]. In Pascal VOC, an
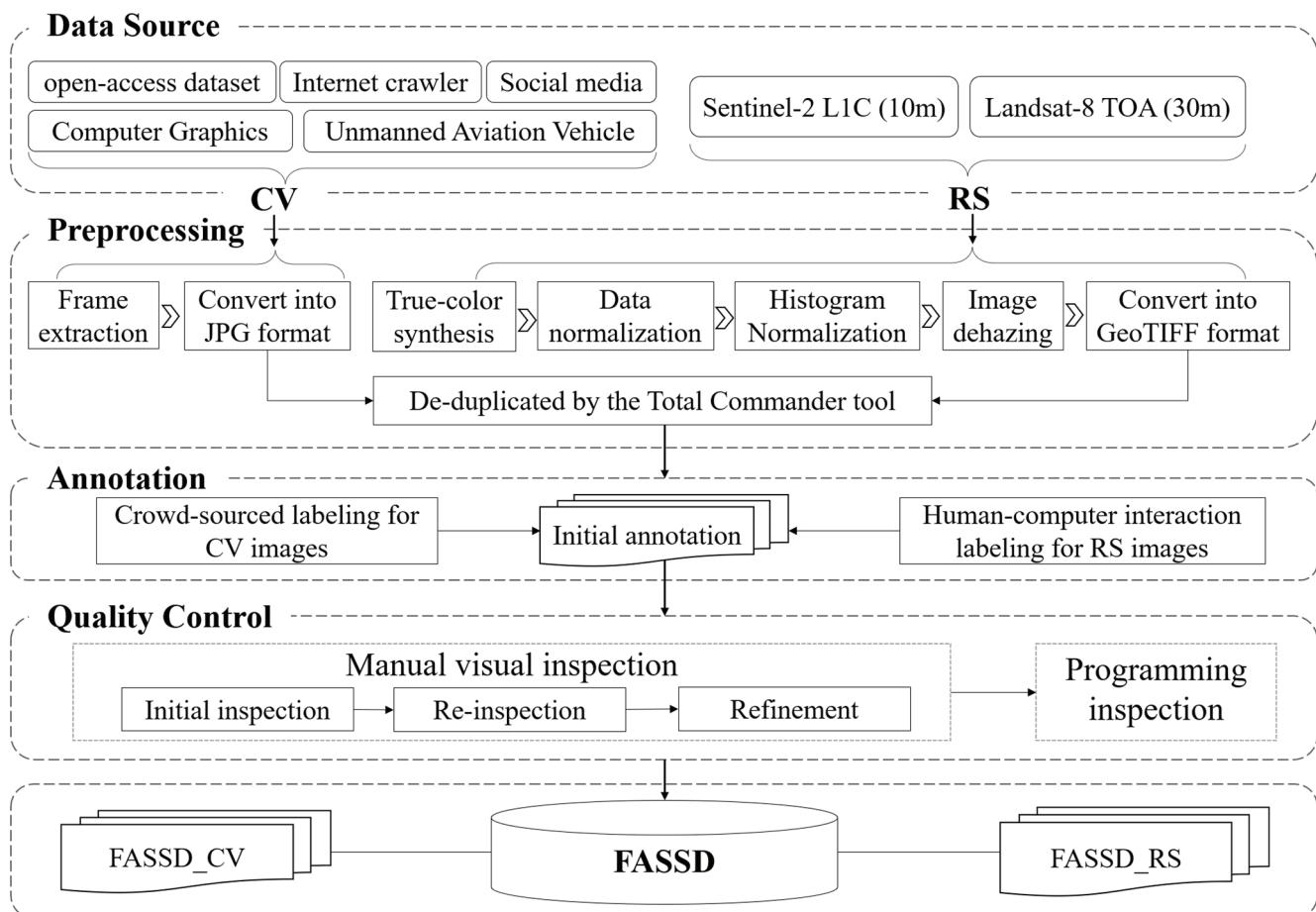
XML annotation is created for each image in the dataset. The "size" keyword is used to store the size information of the corresponding image and the "name" keyword is used to store the category of the object. The upper-left corner and lower-right corner coordinates are used to represent the unique bounding box. Its format can be described as [x_{min}, y_{min}, x_{max}, y_{max}]. In YOLO, an annotation in TXT format is created for each image in the dataset. Its format is [x, y, w, h], which indicates the centroid coordinates, width and height of the bounding box after normalization, respectively.

In addition, the Spatio Temporal Asset Catalog (STAC) provides a common language to describe a range of geospatial information, representing a single spatiotemporal asset as a GeoJSON feature plus datetime and links. Its bounding boxes are represented using either 2D or 3D geometries. Yue et al. (2022) propose a Training data Markup Language (TDML) for producing Machine learning training data, which defines a UML model and encodings consistent with the OGC standards baseline. It supports exchange and retrieve the geospatial machine learning training data in the Web environment, which is consistent with the ubiquitous JSON/XML encoding on the Web. It preserves the basic properties in other common data specifications, while providing more detailed metadata for formalizing the information model of training data. Datasets generated based on these standard data specifications will be more easily adopted and generalized by deep learning researchers.

3 Data generation of FASDD

Considering the limitations of the existing fire datasets in terms of number, modality and visual tasks, this research intends to build a large-scale, multi-modal, multi-resolution, scene-complex, and standardized flame and smoke detection dataset (FASDD), which is suitable for different application fields and compatible with image classification and object detection tasks. Figure 1 illustrates the workflow of generating FASDD. It mainly includes data collection, data preprocessing, data annotation, and quality control. Based on these operating processes, we generate a FASDD_CV dataset for computer vision (CV) tasks, a FASDD_RS dataset for remote sensing (RS) monitoring tasks, and a FASDD dataset for cross-domain object detection tasks compatible with CV and RS. The data generation processes are described in more detail in the following sections.

Figure 1: The workflow for generating FASDD.

3.1 Data source

To build a comprehensive fire dataset for CV tasks, various data sources are used, including existing open-access flame or smoke datasets, social media images, CG (Computer Graphics) paintings, UAV (Unmanned Aerial Vehicle) images, and Internet crawler images. First, ten available open flame or smoke datasets are reused, namely Wildfire Observers and Smoke Recognition Image and video databases (Jakovcevic et al., 2010), Video-based smoke detection image database (Yuan, 2011), Wildfire smoke detection datasets (Ko et al., 2012), the BoWFire (Best of both Worlds Fire detection) dataset (Chino et al., 2015), MIVIA database (Foggia et al., 2015), Fire Detection Image Dataset (Sharma et al., 2017), Smoke Detection Datasets (Zhang et al., 2018), Fire Image Data Set for Dunnings 2018 study (Dunnings et al., 2018), Fire-Smoke-Detection-Dataset (Geng et al., 2020) and the FLAME (Fire Luminosity Airborne-based Machine learning Evaluation) dataset (Shamsoshoara et al., 2021). A large number of source data in these datasets including CG images, UAV images and video frames with good quality, are filtered, extracted and labeled. Some fire-related images are extracted from social media platforms such as TikTok. Objects easily confused with smoke (e.g. dark clouds, shadows, hair and impervious surfaces) and
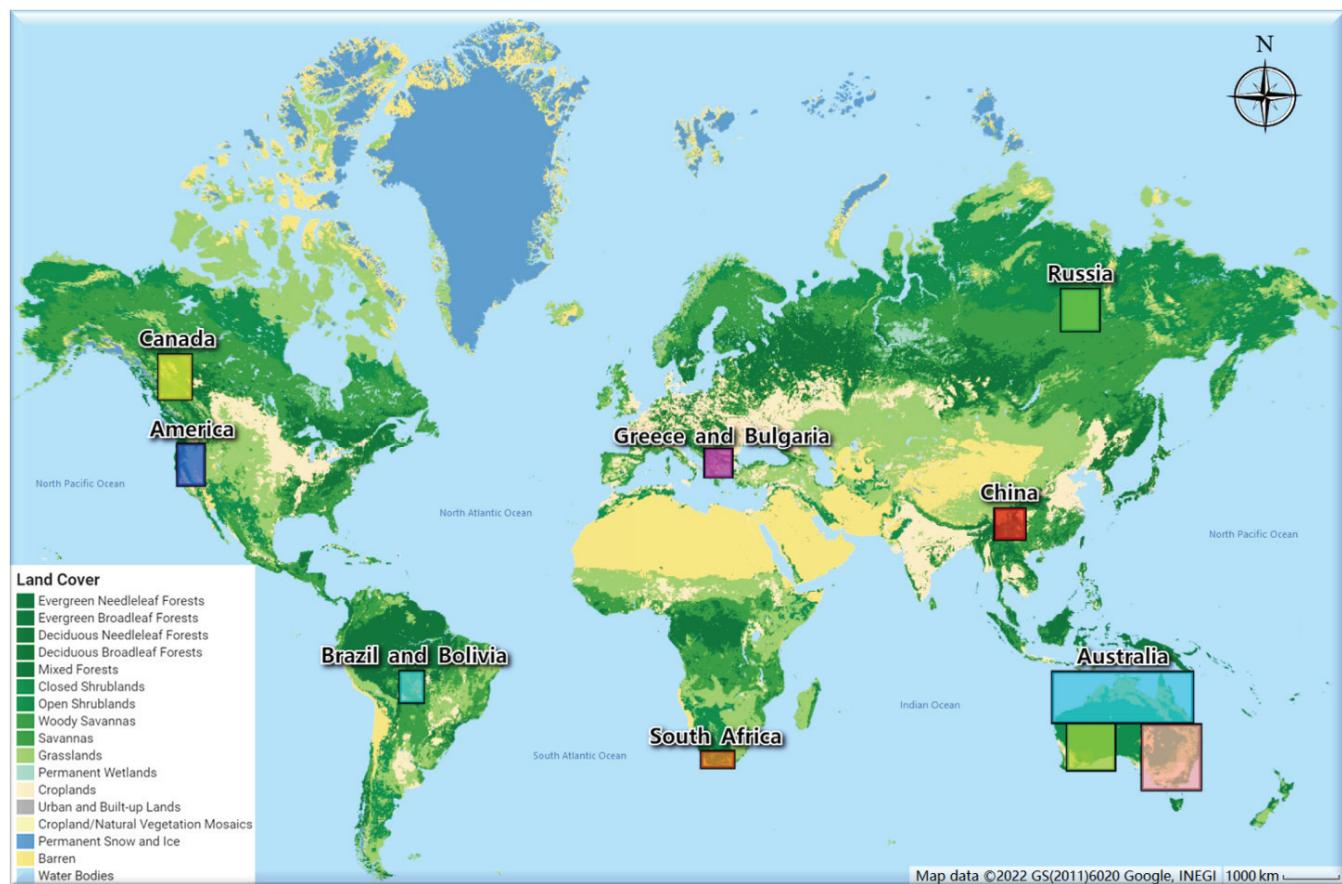
flame (e.g. lights, sunset glow, and reflective clothing) are considered as negative samples. Images about these negative samples are obtained on Internet via Web crawler.

170   In order to produce representative samples of wildfires, ten typical areas (Hu et al., 2021) where wildfires have occurred frequently in recent years are selected (shown in Fig. 2). These regions cover all continents except Antarctica, including Canada, America, Brazil and Bolivia, Greece and Bulgaria, South Africa, China, Russia and Australia. Satellite imagery of these regions captured during fire events are collected from Sentinel-2 with 10m resolution and Landsat-8 with 30m resolution. Table 1 summarizes the details of remote sensing data sources used in this research. Since the atmospheric

175   correction process may lead to the problem of missing pixels around the smoke and clouds in surface reflection imagery, we make use of Sentinel-2 and Landsat-8 data product that are not corrected for atmospheric conditions, namely Sentinel-2 L1C (Level-1C) and Landsat-8 TOA (top-of-atmosphere), to generate FASDD_RS. A total of 310,280 remote sensing images with cloudy pixel percentage below 5% are collected. The RS image sizes range from 1000×1000 to 2200×2200.

180   **Figure 2: The typical areas of fire events around the world. The base map (map data from Google Earth Engine © Google Services 2022) shows MODIS global land cover types at yearly intervals (Friedl and Sulla-Menashe, 2020) distributed by NASA's Land Processes Distributed Active Archive Center.**

Table 1 The details of data collection for typical fire events around the world

Region	Continent	Time range	Spatial range	Data source	Number	Resolution
Canada	North America	2018.08.05 - 2018.08.15	[-129.00, 58.90], [-129.00, 53.06], [-120.08, 53.06], [-120.08, 58.90]	Sentinel-2, L1C	5764	10m
America	North America	2018.11.05 - 2018.11.15	[-123.50, 44.62], [-123.50, 37.37], [-118.16, 37.37], [-118.16, 44.62]	Sentinel-2, L1C	8437	10m
Brazil and Bolivia	South America	2019.08.15 - 2019.08.25	[-62.30, -11.18], [-62.30, -18.49], [-58.68, -18.49], [-58.68, -11.18]	Sentinel-2, L1C	6977	10m
Greece and Bulgaria	Europe	2018.07.15 - 2018.07.25	[19.65, 43.16], [19.65, 38.59], [25.08, 38.59], [25.08, 43.16]	Sentinel-2, L1C	10725	10m
South Africa	Africa	2018.10.20 - 2018.10.30	[18.76, -31.84], [18.76, -34.58], [25.92, -34.58], [25.92, -31.84]	Sentinel-2, L1C	9573	10m
China	Asia	2020.03.30 - 2020.04.05	[101.28, 28.25], [101.28, 27.84], [101.65, 27.84], [101.65, 28.25]	Sentinel-2, L1C	624	10m
Russia	Europe	2018.07.15 - 2018.07.25	[118.05, 66.69], [118.05, 64.81], [122.26, 64.81], [122.26, 66.69]	Sentinel-2, L1C	2111	10m
Australia	Oceania	2019.07.01 - 2020.02.20	[113.10, -10.81], [113.10, -23.77], [151.16, -23.77], [151.16, -10.81]	Sentinel-2, L1C	182932	10m
			[137.37, -23.68], [137.37, -38.99], [153.27, -38.99], [153.27, -23.68]	Landsat-8, TOA	52669	30m
			[117.41, -23.84], [117.41, -34.41], [129.89, -34.41], [129.89, -23.84]	Landsat-8, TOA	30468	30m

185 **3.2 Data preprocessing**

To ensure the consistency and standardization of FASDD, some basic preprocessing steps on source data shall be conducted before data annotation. For video data, key frame extraction is performed and images are sampled in a step of 30 frames to ensure the difference between samples. Then all CV images (including images extracted from videos) are converted into JPEG format files. For remote sensing imagery, additional processing steps are required including true-color synthesis, data

190 normalization, and image dehazing. All remote sensing images are synthesized into true-color images for human interpretation. Pixel values are normalized to the range of 0-255. These preprocessing steps allow them to be suitable for general flame and smoke detection models. Then, histogram normalization and dehazing are performed to adjust the image color components and improve the image clarity. And all remote sensing images are saved as GeoTIFF format files. In the

end, all images with the same content are de-duplicated based on the Total Commander tool (Total Commander, 2022) to
195   ensure the difference and uniqueness of image features in the dataset.

3.3 Data annotation

For CV training data annotation, all selected images are distributed to more than 70 volunteers in the field of fire detection
for collaborative labeling in a crowd-sourced manner. Volunteer annotators are asked to label flame and smoke objects in
images using non-directional minimum bounding rectangle. Although data are labeled offline with the LabelImg tool, some
200   basic annotation rules are formulated to standardize the labeling process. The annotation rules can be summarized as follows:

- A flame or a smoke object that is partially occluded but obviously connected is regarded as a separate object;
- Multiple tiny objects clustered together are considered to be a particular object;
- Flame or smoke with significantly different colors are not considered to be the same object;
- Objects smaller than 10×10 pixels and without apparent flame or smoke characteristics are ignored;
205   - Inconspicuous reflections of flame and smoke on smooth surfaces such as water shall be ignored;
- Small objects with prominent characteristics shall be not omitted;
- Images with too low resolution or with inconspicuous flame and smoke features shall be deleted.

For RS training data annotation, we adopt a semi-automatic way to annotate RS images with human-computer interaction.
First, target images which may contain flame and smoke objects or confusing objects are manually searched and screened.
210   All the target images are distributed to a small group of trained annotators to produce positive samples. Meanwhile, a flame
and smoke detection model trained on existing FASDD_CV is employed to predict semantic tags of target images. Those
images with confidence greater than 80% are further screened out from the inference results, and labels in those images
similar to flame and smoke are manually annotated as negative samples. In the annotation process, spatial information of all
remote sensing images, including longitude, latitude, and projection information, are retained for the localization and
215   tracking of forest fire events. Finally, 5,773 images are annotated based on human-computer interaction.

The flame and smoke objects in FASDD are given the labels "fire" and "smoke" for the object detection task, respectively.
Annotation files in four kinds of formats are provided in FASDD, i.e., the JSON format defined by the TDML (Yue et al.,
2022), the XML format adopted by the PASCAL VOC (Everingham et al., 2015) dataset, the JSON format adopted by the
Microsoft COCO (Lin et al., 2014) dataset, and the text format adopted by models of YOLO (Redmon et al., 2016) series.
220   Examples of four annotation formats are displayed in the attached file. Since all images could be classified into four
semantic categories, i.e. "Fire", "Smoke", "FireAndSmoke", and "NeitherFireNorSmoke", the category label is added to each
image filename as prefix. With such category prefixes, FASDD could also be used to train fire scene classification models.

3.4 Quality control

To ensure the quality of the dataset, we develop a set of quality control procedures. On the one hand, three-stage manual
225   visual inspection procedures are designed after obtaining the initial annotation files of the dataset, i.e., initial inspection, re-

inspection, and refinement, to correct unconfident data. In the initial inspection stage, every two annotators are assigned into one group to cross-check and modify the annotation files against each other, which helps find out inconsistent labels between different interpreters and reduce cognitive biases in crowdsourcing annotations. In the re-inspection stage, a small group of quality inspectors are trained to audit the results from the initial inspection stage to eliminate omission errors and fine-tune

230   the position, category, width, and height of bounding boxes. In the refinement stage, we invite well-trained domain experts to resolve annotation conflicts from the initial stage and relabel difficult-to-determine labeling cases from the previous stages. On the other hand, we introduce a programming inspection procedure after manual visual inspection procedures. The programming inspection procedure performs final data cleaning on annotation files using annotation checking code. The code could automatically modify empty, duplicated or range overflow bounding boxes, and misclassified or misspelt labels

235   to prevent invalid and omitted values that are not easily detectable by humans. After these inspection steps, the consistency and standardization of annotation files can be ensured as much as possible.
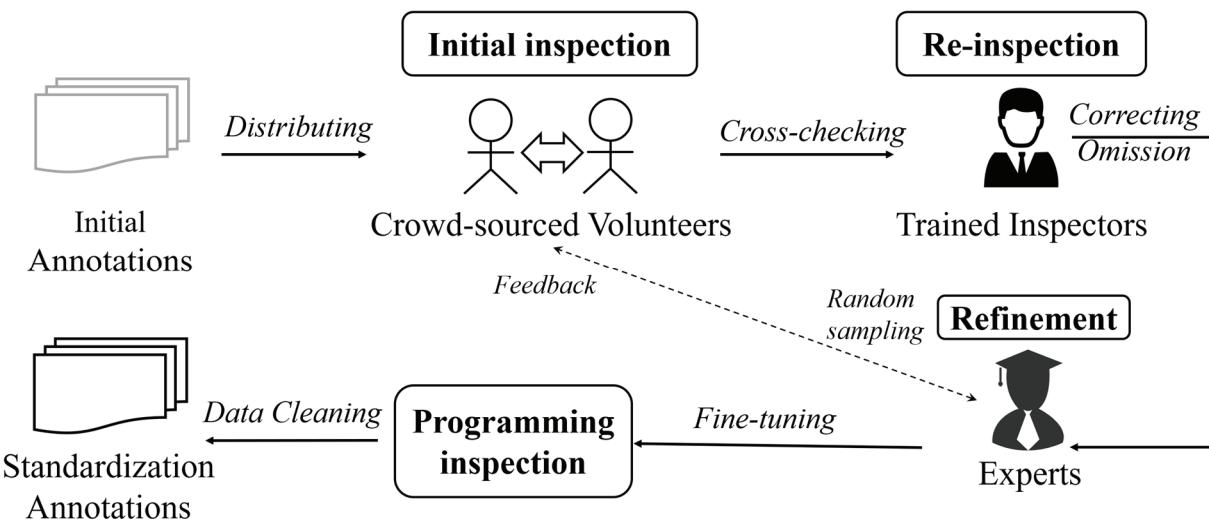
Figure 3: The quality control flowchart

3.5 Dataset characteristics and values

240   FASDD contains fire, smoke, and confusing non-fire/non-smoke images acquired at different distances (near and far), different scenes (indoor and outdoor), different light intensities (day and night), and from various visual sensors (surveillance cameras, UAV, and satellites). A total of 101,087 samples are produced, of which 59,177 are annotated as positive samples, and 41,910 are labelled as negative samples. Some example images of FASDD are shown in Fig. 4. There are 82,666 flame object instances and 57,742 smoke object instances labelled in the entire dataset. FASDD consists of two sub-datasets, a

245   computer vision dataset (i.e. FASDD_CV) consisting of 95,314 general computer vision (CV) samples, and a remote sensing dataset (i.e. FASDD_RS) consisting of 5,773 remote sensing (RS) samples. FASDD_CV contains 73,297 fire instances and 53,080 smoke instances. The size of CV images spans a relatively large range, with a width range of 78~10,600 pixels and a

height range of 68~8,858 pixels. The image aspect ratios are also quite different, widely ranging from 1:6.6 to 1:0.18. FASDD_RS contains 9,369 fire instances and 4,662 smoke instances. The sizes of remote sensing images are mainly
250   distributed around 1,000×1,000 or 2,200×2,200 pixels.
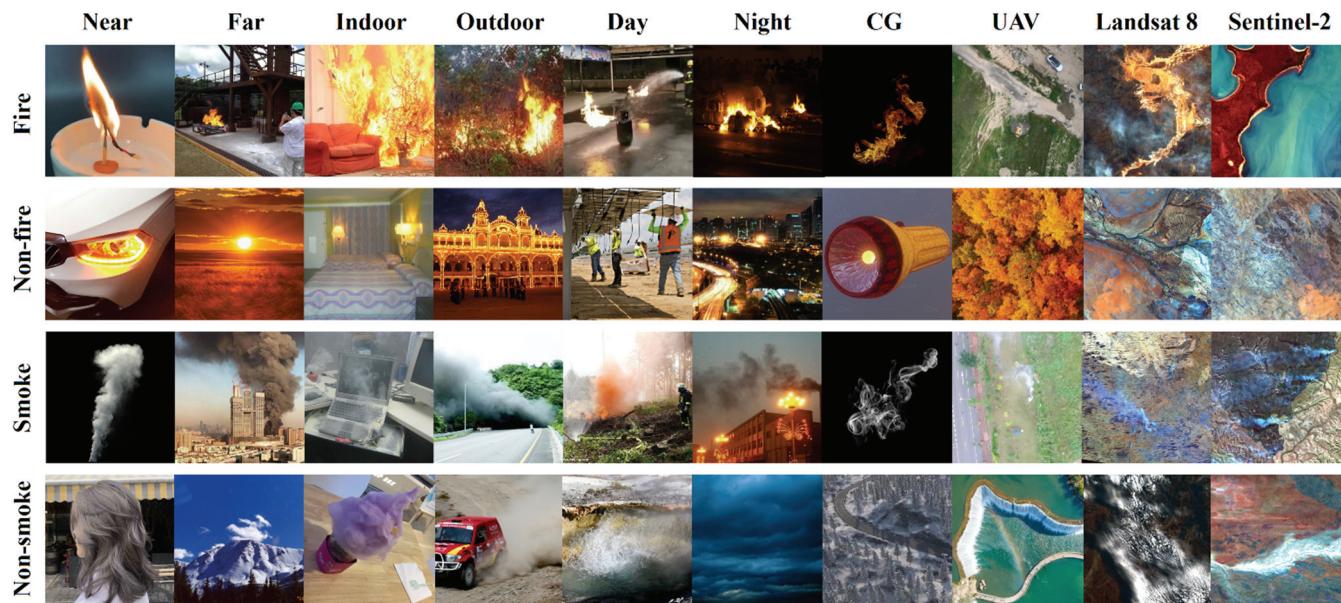
Figure 4: The example images in FASDD. CV images are from open-access datasets (Chino et al., 2015; Sharma et al., 2017; Geng et al., 2020). RS images are from Landsat-8 TOA and Sentinel-2 L1C.

Compared with existing fire datasets including FLAME (Shamsoshoara et al., 2021), MIVIA (Foggia et al., 2015) and
255   BoWFire (Chino et al., 2015), FASDD has the following remarkable characteristics.

(1) Large Scale. FASDD consists of more than 100,000 images and 140,000 object instances that are manually labelled with bounding boxes. To the best of our knowledge, it is the most versatile, comprehensive, and publicly available dataset for fire detection.

(2) Rich sample variations. The proposed FASDD dataset holds rich variations in image size, resolution, illumination (day
260   and night), scene (indoor and outdoor), image range (far and near), sensor (surveillance cameras, UAV sensors, and satellite), and data source (Internet, social media, and open-access fire datasets). Such image variations will help enhance the robustness of models.

(3) High intra-class diversity and some inter-class similarity. Due to the characteristics of growth, disorder, color diversity, and intensity variability of flame and smoke, objects in the same category have different sizes, postures, and colors. There
265   are also some similarities between flame and smoke, such as the red smoke by the glow of flame looks like the flame.

(4) Small objects of flame and smoke. It is well known that small object detection is a challenging problem in deep learning research related to computer vision. FASDD contains a large number of small flame and smoke objects, especially flame objects from remote sensing imagery and far-field wildfire images.

(5) Geo-referenced images. Compared with traditional CV datasets, FASDD contains a number of geo-referenced training
270 images. The location information in remote sensing images can be used to detect or infer the location of fire events in time.

4 Evaluation and application

4.1 Experiment Setup

In our experiment, we select half of the dataset for training, 1/3 for validation, and 1/6 for test. Four classical models with
significant architectural differences are selected for performance evaluation, including the two-stage Faster-RCNN (Ren et
275 al., 2015), the one-stage anchor-free GFL (Li et al., 2020), the anchor-based YOLOv5x (Jocher et al., 2021), and the Swin
Transformer (Liu et al., 2021) that achieves state-of-the-art (SOTA) performance on the COCO dataset. We use the same
training configuration for all models participating in the evaluation to ensure the fairness of performance comparison. All
models are trained from scratch without using pre-trained weight files. The only exception is that YOLOv5x uses an image
size 960×960, while other models use the image size from 1333×480 to 1333×800. Other parameters are consistent for the
280 four models, including epoch 36 and batch size 2. In terms of GPU devices, all models for are trained, validated, and tested
on an NVIDIA GeForce RTX 3090 with 24GB memory.

4.2 Evaluation metrics

Four metrics are used to quantitatively evaluate the accuracy of the model prediction results, including Precision, Recall, AP
(Average Precision), and mAP (mean Average Precision). Precision represents the ratio of the correct prediction box to all
285 prediction boxes. Recall represents the ratio of the correct prediction box to all ground-truth boxes. AP represents the area
under the curve (AUC) of Precision-Recall for each class in the dataset. mAP represents the AP mean value of all class. We
select the mAP@0.5, a more representative mAP indicator, as the primary reference metric of model accuracy. The
mAP@0.5 refers to mAP when the IoU between prediction and ground-truth boxes is not less than 50%, which is usually
used to evaluate the overall performance of models. Precision and Recall are calculated as shown in Eq. (1) and (2):

$$Precision = \frac{TP}{TP + FP} \tag{1}$$

$$Recall = \frac{TP}{TP + FN} \tag{2}$$

290 where, TP represents the number of prediction boxes when the IoU between prediction and ground-truth boxes is not less
than 0.5. FP represents the number of prediction boxes when the IoU between the prediction and ground-truth boxes is less
than 0.5. FN represents the number of the ground-truth boxes missed from detection.

4.3 Performance evaluation

We train Faster-RCNN, GFL, Swin Transformer and YOLOv5x models on FASDD_CV, FASDD_RS and FASDD, and
295 evaluate and compare the accuracy of these classic object detection models based on validation set and test set in the above
three datasets, respectively. Table 2 shows the accuracy evaluation results of classical models on FASDD_CV, FASDD_RS
and FASDD.

Table 2: Accuracy evaluation of classic object detection models

Datasets	Method	epoch	Validation			Test		
			AP_{fire} (%)	AP_{smoke} (%)	mAP@0.5 (%)	AP_{fire} (%)	AP_{smoke} (%)	mAP@0.5 (%)
FASDD_CV	Faster-RCNN	36	48.20	56.90	52.55	67.40	55.20	61.26
	GFL	36	56.60	69.00	62.82	72.70	73.10	72.90
	Swin Transformer	36	65.00	**74.60**	69.79	81.50	76.10	78.77
	YOLOv5x	36	**70.96**	73.29	**72.13**	**86.48**	**81.66**	**84.07**
FASDD_RS	Faster-RCNN	36	25.80	31.60	28.66	24.3	39.8	32.05
	GFL	36	34.00	36.90	35.46	33.5	46.6	40.08
	Swin Transformer	36	**43.40**	**56.80**	**50.10**	**41.00**	**65.00**	**53.01**
	YOLOv5x	36	37.35	45.93	41.64	33.42	49.35	41.39
FASDD	Faster-RCNN	36	44.30	53.70	49.00	59.00	51.50	55.24
	GFL	36	53.60	67.10	60.35	65.80	70.60	68.20
	Swin Transformer	36	58.90	**72.20**	65.55	71.20	71.20	73.20
	YOLOv5x	36	**67.80**	72.10	**69.94**	**79.14**	**79.17**	**79.15**

In the evaluation results on FASDD_CV, the overall accuracy of Faster-RCNN, GFL, YOLOv5x, and Swin Transformer
300 is gradually increasing. Among them, the Faster-RCNN model achieves only 52.55% validation mAP@0.5 and 61.26% test
mAP@0.5 on FASDD_CV. The GFL and Swin Transformer models exhibit a good performance, and the Swin model
achieves the highest validation accuracy of 74.60% on the AP_{smoke} metric. The YOLOv5x model shows the best performance,
achieving the highest accuracy in all metrics except AP_{smoke}, particularly the 84.07% mAP@0.5 accuracy on the test set.
Considering the evaluation results again, the worst performing Faster-RCNN also achieves an evaluation accuracy higher
305 than 60% on FASDD_CV, which is partly due to the contribution of the large-scale sample of FASDD_CV.

In the evaluation results on FASDD_RS, the overall accuracy of all models is significantly lower than that on
FASDD_CV, which demonstrates the difficulty of fire detection on Remote Sensing images. Among them, the Faster-RCNN
exhibits the lowest model performance. Compared with the Faster-RCNN model, GFL exhibits performance improvement to
some extent. And YOLOv5x outperforms the GFL on both the validation and test sets. The Swin Transformer model
310 achieves the best performance with 56.70% and 53.01% mAP@0.5 on the validation and test set, respectively. This may be
attributed to its transformer structure, which is better at capturing global contextual information and large-scale spatial

relationships. Some smoke areas in remote sensing images of large fire are relatively large, so the Swin Transformer model achieves the most advanced performance on FASDD, especially on the AP_{smoke} metric.

In the evaluation results on FASDD, the two-stage object detection model, Faster-RCNN, shows the lowest performance on both FASDD validation and test set with 49.00% and 55.24% mAP@0.5 respectively. Compared with Faster-RCNN, the one-stage anchor-free GFL model obtains 11.35% and 12.96% mAP@0.5 performance gains on validation (60.35%) and test (68.20%) sets. Compared with Faster-RCNN and GFL, Swin Transformer has significant performance improvement. Moreover, its validation set accuracy (65.55%) and test set accuracy (73.20%) are the closest to the accuracy evaluation results of YOLOv5x, showing a pretty competitive accuracy evaluation result. The anchor-based YOLOv5x exhibits state-of-the-art performance on FASDD, achieving the highest 69.94% validation accuracy and 79.15% test accuracy on the mAP@0.5 metric. The accuracy of the Swin Transformer is slightly lower than that of YOLOv5x. The reason may be that the parameter configuration and training strategy of the two models are only as consistent as possible but not entirely consistent, which may lead to a loss of comparability to some extent.
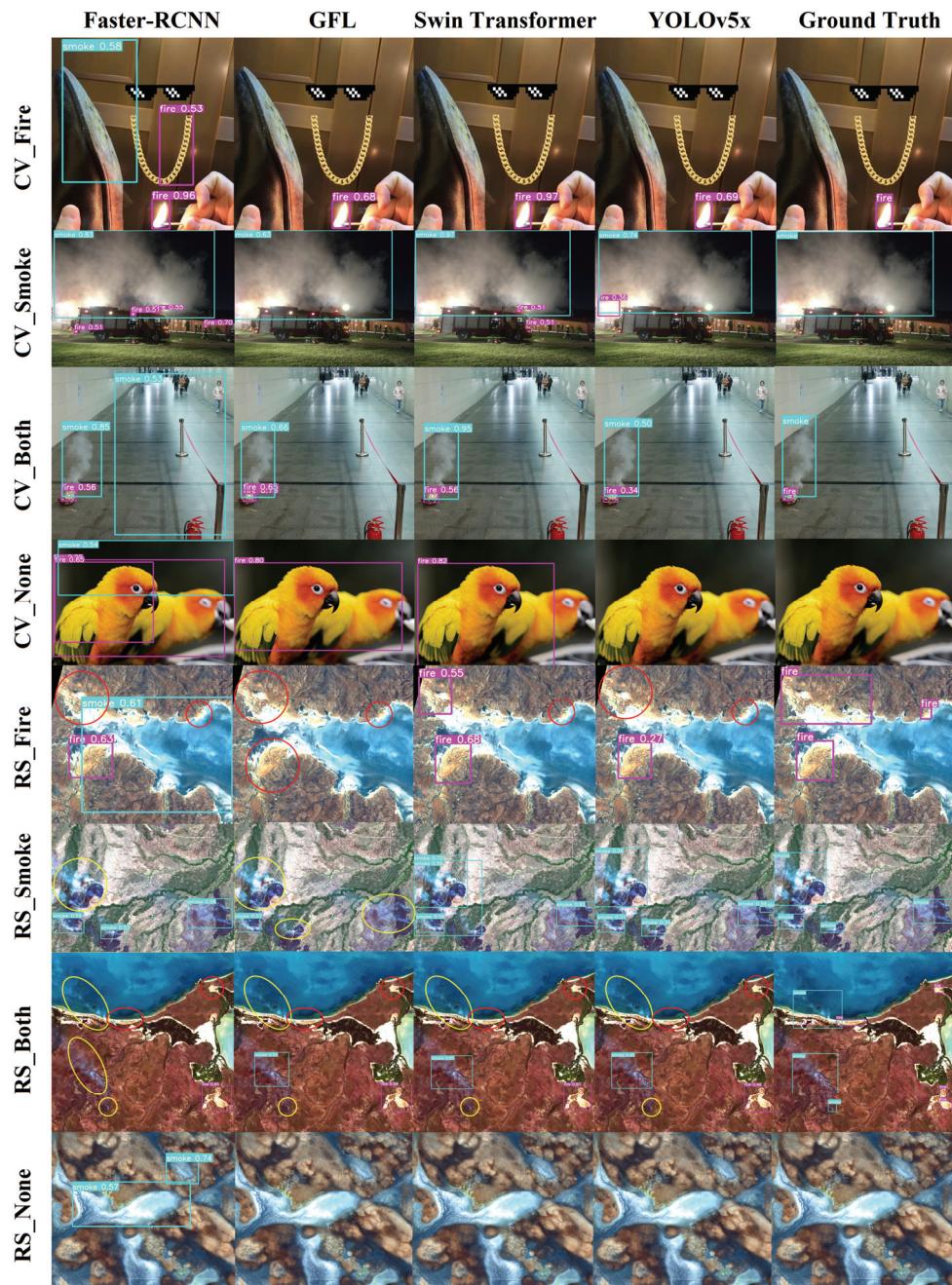
Experiments show that the detection accuracy of the classical object detection model on FASDD_CV is generally better than that on FASDD_RS. In terms of overall assessment results, the models also demonstrate good detection performance on FASDD that integrates cross-domain data (CV and RS). This indicates that the pre-trained model trained on FASDD can achieve good accuracy, generalizability, and transfer learning capability on the cross-domain object detection task. However, FASDD is still challenging and there is sufficient space to improve its detection accuracy. It can be used to assist researchers in developing more targeted and robust algorithms to promote new developments in fire detection. Moreover, based on FASDD, we can provide pre-trained large models with better generalization performance for downstream tasks such as object detection and semantic segmentation.

4.4 Visual results

Figure 5 shows the prediction results of classic object detection models on FASDD_CV and FASDD_RS example images, and compares them on four categories of fire images, i.e. Fire, Smoke, FireAndSmoke, and NetherFireNorSmoke. In the CV_Fire results, Faster-RCNN incorrectly detects a gold necklace as flame and a black shoe as smoke. In the CV_Smoke results, the lights on the fire truck and helmets of firefighters bring challenges to Faster-RCNN and Swin Transformer. In the CV_Both results, Faster-RCNN incorrectly detects grey shadows on the ground as smoke. In the CV_None results, Faster-RCNN, GFL, and SwinTransformer incorrectly detect colored parrots as flame, and Faster-RCNN detects black backgrounds as smoke. In the RS_Fire results, all models have different degrees of omission errors. In particular, GFL does not detect the existence of flame objects at all, and Faster-RCNN incorrectly detects large areas of water as smoke. In terms of the RS_Smoke, Faster-RCNN and GFL show obvious problems of missed detection. In RS_Both, all models show missed detection of flame and smoke objects, and the missed detection of Faster-RCNN is severe. In the RS_None category, only the Faster-RCNN model incorrectly detects the dark blue surface as smoke, and none of the other models shows the false alarm. To sum up, in terms of image features, the significance level of flame and smoke features in FASDD_RS images is

345   slightly less than that of FASDD_CV images, and the flame in FASDD_RS image is easily confused with remote sensing ground objects or various scenes in reality. That is to say, detecting flame in remote sensing images is much more complex and challenging than in CV images.

Figure 5: The visual result of classical object detection models on the example images. Red circles indicate omitted flame, and
350   **yellow circles indicate omitted smoke. "Both" represents images of the "FireAndSmoke" category, and "None" means images of**

the "NetherFireNorSmoke" category. CV images are from open-access datasets (Chino et al., 2015; Dunnings et al., 2018; Geng et al., 2020). RS images are from Landsat-8 TOA and Sentinel-2 L1C.

In terms of model performance, the false alarm rate of Faster-RCNN is higher than other models, and the model has the worst performance. The notable feature of GFL is its highly-missed detection rate on FASDD_RS. Swin Transformer also

355 shows the false alarm and missed detection, yet the overall detection effect is good. YOLOv5x can achieve a satisfactory detection effect except that few missed detections on FASDD_RS. These results are obtained under the small batch size and epoch training configuration. Better detection results are possibly achieved using the optimized algorithms, the tuned parameters, or an extended training period.

4.5 Application in wildfire location

360 We apply the above classical methods to fire localization experiments in wildfire scenarios from remote sensing images. The latitude and longitude coordinates of the predicted boxes are used to verify the positioning accuracy of these methods. First, the coordinate system of the RS_Smoke image in Fig. 5 is converted to WGS84-based GPS coordinates. Then, inferences are performed on the georeferenced RS_Smoke image withfour trained object detection models respectively. Finally, the positions of all prediction boxes are converted into the form of latitude and longitude coordinates.

365   **Table 3: Comparison of coordinates between prediction and ground truth boxes**

Box	Model	Top Left Coordinate	Bottom Right Coordinate	Centroid Distance Bias (m)	IoU
	Faster-RCNN	[142.5292, -13.8503]	[142.5413, -13.8578]	452.22	0.33
	GFL	-	-	-	-
Box1	Swin Transformer	-	-	-	-
	YOLOv5x	**[142.5283, -13.8507]**	**[142.5405, -13.8564]**	**360.03**	**0.37**
	Ground Truth	[142.5251, -13.8453]	[142.5406, -13.8559]	0.00	1.00
	Faster-RCNN	[142.5826, -13.8343]	[142.5971, -13.8477]	646.24	0.49
	GFL	-	-	-	-
Box2	Swin Transformer	[142.5831, -13.8347]	[142.6084, -13.8486]	**31.62**	0.90
	YOLOv5x	**[142.5836, -13.8341]**	**[142.6070, -13.8483]**	63.25	**0.93**
	Ground Truth	[142.5841, -13.8344]	[142.6076, -13.8483]	0.00	1.00
	Faster-RCNN	-	-	-	-
	GFL	-	-	-	-
Box3	Swin Transformer	[142.4985, -13.8446]	[142.5161, -13.8555]	**36.06**	0.82
	YOLOv5x	**[142.4999, -13.8452]**	**[142.5159, -13.8555]**	65.19	**0.87**
	Ground Truth	[142.4997, -13.8448]	[142.5155, -13.8548]	0.00	1.00
	Faster-RCNN	-	-	-	-
	GFL	[142.4961, -13.8144]	[142.5223, -13.8535]	917.40	0.52
Box4	Swin Transformer	[142.4965, -13.8104]	[142.5306, -13.8437]	127.48	0.83
	YOLOv5x	**[142.4976, -13.8126]**	**[142.5291, -13.8401]**	**68.01**	**0.89**
	Ground Truth	[142.4968, -13.8113]	[142.5288, -13.8410]	0.00	1.00

Table 3 compares the geographic coordinates (top left and bottom right), centroid distance bias and IoU between the prediction boxes and ground truth boxes of the RS_smoke image. "-" indicates the missed detection boxes, and the redundant boxes of false alarm is not added to the table. Among them, GFL misses three bounding boxes, Faster-RCNN misses two bounding boxes, Swin Transformer misses one bounding box, and YOLOv5x can detect all the bounding boxes. Compared
370 with the detection results of other models, the predicted geographic coordinates of the YOLOv5x model and the ground-truth boxes are closer, showing a good fire site localization effect. In terms of the centroid distance, the prediction box centroids of both Faster-RCNN and GFL are relatively far from the ground truth centroids, and the prediction box centroids of Swin Transformer and YOLOv5x are relatively closer to the ground truth centroids. In terms of the IoU, Swin Transformer and YOLOv5x also exhibit good results around 90% on most of the prediction boxes. In particular, YOLOv5x achieve the
375 highest IoU between all prediction boxes and ground truth boxes. The above comparison results show that YOLOv5x model trained on FASDD helps to accurately locate and track wildfire sites in remote sensing images. This has practical significance for detecting and monitoring large-scale forest fires using in-orbit satellites.

5 Data availability

FASDD is freely available from the Science Data Bank website at https://doi.org/10.57760/sciencedb.j00104.00103 (Wang
380 et al., 2022). There are a total of three compressed files, FASDD_CV.zip, FASDD_RS.zip and FASDD.zip represent the CV dataset, the RS dataset and the full dataset composed of CV and RS respectively. Each zip file contains an "images" folder for storing data and an "annotations" folder for storing labels. The 'annotations' folder consists of label files in four formats: VOC, COCO, YOLO, and TDML. In each format of labels, the dataset is divided into training, validation, and test sets with a ratio of 1/2, 1/3, and 1/6. The prefixes of image and label names are divided into "Fire", "Smoke", "FireAndSmoke", and
385 "NeitherFireNorSmoke", which represent different categories of data for classification tasks. The labels contain the classes "fire" and "smoke" to represent two common objects in fire images for object detection tasks.

6 Conclusion

This paper presents an open-access 100,000-level Flame and Smoke Detection Dataset (FASDD). To the best of our knowledge, it is the largest fire detection dataset with the most variety of scenes, the highest heterogeneity, and the most
390 significant difference in feature distribution. FASDD is compatible with image classification and object detection tasks. It provides four annotation files to enable out-of-the-box training samples for deep learning models. Especially, the use of TDML annotations provides a reference for the application of upcoming OGC training data standard in the future. FASDD has significant heterogeneity and challenges, laying a solid data foundation for future fire detection research. Based on the proposed dataset, we perform extensive performance evaluations and comparisons using multiple classic object detection
395 models. The results show that YOLOv5x model exhibits state-of-the-art performance with the highest test set accuracy close

to 80%. That is to say, the trained YOLOv5x model can play a considerable role in the early warning and detection of urban fires or forest fires. The application in wildfire location finds that YOLOv5x model trained on FASDD can achieve high-quality location results. The model can be adapted to any other regional and global scales fire scenarios, which can provide an important reference for government decision-making and fire rescue. However, there is still room to improve the accuracy

400 of fire detection with fine-tuned models. In particular, advanced wildfire detection models need to be developed for the challenging task of recognizing fire on remote sensing imagery. In the future, vision-based models trained on FASDD can also be combined with smoke sensors in practical applications for more accurate fire detection.

Author contributions

MW, LJ and PY conceived the study. MW wrote the first draft of the manuscript and managed data archiving. LJ and PY

405 provided input on the overall methodology and participated in drafting the manuscript. DY and TT participated in the data collection, data annotation, and quality control of the dataset. All authors discussed the results and commented on the manuscript.

Competing interests

The authors declare that they have no conflict of interest.

410 **Acknowledgements**

We appreciate the volunteer annotators who contributed to the establishment of this dataset. We greatly thank the free access to the Landsat data provided by the USGS; the Sentinel data provided by the European Space Agency; the MCD12Q1 product provided by NASA's Land Processes Distributed Active Archive Center, and the fire detection datasets provided by many researchers (Jakovcevic et al., 2010; Yuan, 2011; Ko et al., 2012; Chino et al., 2015; Foggia et al., 2015; Sharma et al.,

415 2017; Zhang et al., 2018; Dunnings et al., 2018; Geng et al., 2020; Shamsoshoara et al., 2021). We would like to thank the Google Earth Engine team for sharing geospatial cloud platform, the Ultralytics team for sharing YOLOv5 code (https://github.com/ultralytics/yolov5, last access: 16 November 2022), and the GitHub user K-H-Ismail for sharing Faster-RCNN, GFL and Swin transformer code (https://github.com/SwinTransformer/Swin-Transformer-Object-Detection, last access: 16 November 2022).

References

Bernal, J., Histace, A., Masana, M., Angermann, Q., Sánchez-Montes, C., Rodríguez de Miguel, C., Hammami, M., García-Rodríguez, A., Córdova, H., Romain, O., Fernández-Esparrach, G., Dray, X., and Sánchez, F. J.: GTCreator: a flexible annotation tool for image-based datasets, Int J CARS, 14, 191-201, https://doi.org/10.1007/s11548-018-1864-x, 2019.

Brushlinsky N., Sokolov S., Wagner P., and Messerschmidt B.: World Fire Statistics, Ph.D., CTIF Center for Fire Statistics, 65 pp., https://ctif.org/sites/default/files/2022-08/CTIF_Report27_ESG_0.pdf, 2022.

Bu, F., and Gharajeh, M. S.: Intelligent and vision-based fire detection systems: A survey, Image and Vision Computing, 91, 103803, https://doi.org/10.1016/j.imavis.2019.08.007, 2019.

Calderara, S., Piccinini, P., and Cucchiara, R.: Smoke Detection in Video Surveillance: A MoG Model in the Wavelet Domain, in: Computer Vision Systems, Berlin, Heidelberg, 119-128, https://doi.org/10.1007/978-3-540-79547-6_12, 2008.

Cheng, S., Ma, J., and Zhang, S.: Smoke detection and trend prediction method based on Deeplabv3+ and generative adversarial network, JEI, 28, 033006, https://doi.org/10.1117/1.JEI.28.3.033006, 2019.

Chi, R., Lu, Z.-M., and Ji, Q.-G.: Real-time multi-feature based fire flame detection in video, IET Image Processing, 11, 31-37, https://doi.org/10.1049/iet-ipr.2016.0193, 2017.

Chino, D. Y. T., Avalhais, L. P. S., Rodrigues, J. F., and Traina, A. J. M.: BoWFire: Detection of Fire in Still Images by Integrating Pixel Color and Texture Analysis, in: 2015 28th SIBGRAPI Conference on Graphics, Patterns and Images, 2015 28th SIBGRAPI Conference on Graphics, Patterns and Images, 95-102, https://doi.org/10.1109/SIBGRAPI.2015.19, 2015.

Chowdary, V., Gupta, M., and Singh, R.: A Review on Forest Fire Detection Techniques: A Decadal Perspective, International Journal of Engineering & Technology, 7, 1312, https://doi.org/10.14419/ijet.v7i3.12.17876, 2018.

Tzutalin, D.: LabelImg Is a Graphical Image Annotation Tool and Label Object Bounding Boxes in Images, GitHub [data set], https://github.com/tzutalin/labelImg, 2015.

Dimitropoulos, K., Barmpoutis, P., and Grammalidis, N.: Spatio-Temporal Flame Modeling and Dynamic Texture Analysis for Automatic Video-Based Fire Detection, IEEE Transactions on Circuits and Systems for Video Technology, 25, 339-351, https://doi.org/10.1109/TCSVT.2014.2339592, 2015.

Dua, M., Kumar, M., Singh Charan, G., and Sagar Ravi, P.: An Improved Approach for Fire Detection using Deep Learning Models, in: 2020 International Conference on Industry 4.0 Technology (I4Tech), 2020 International Conference on Industry 4.0 Technology (I4Tech), 171-175, https://doi.org/10.1109/I4Tech48345.2020.9102697, 2020.

Dunnings, A. J., and Breckon, T. P.: Experimentally Defined Convolutional Neural Network Architecture Variants for Non-Temporal Real-Time Fire Detection, in: 2018 25th IEEE International Conference on Image Processing (ICIP), 2018 25th IEEE International Conference on Image Processing (ICIP), 1558-1562, https://doi.org/10.1109/ICIP.2018.8451657, 2018.

Dutta, A., and Zisserman, A.: The VIA Annotation Software for Images, Audio and Video, in: Proceedings of the 27th ACM International Conference on Multimedia, New York, NY, USA, 2276-2279, https://doi.org/10.1145/3343031.3350535, 2019.

Everingham, M., Eslami, S. M. A., Van Gool, L., Williams, C. K. I., Winn, J., and Zisserman, A.: The Pascal Visual Object Classes Challenge: A Retrospective, Int J Comput Vis, 111, 98-136, https://doi.org/10.1007/s11263-014-0733-5, 2015.

Fiedler, N., Bestmann, M., and Hendrich, N.: ImageTagger: An Open Source Online Platform for Collaborative Image Labeling, in: RoboCup 2018: Robot World Cup XXII, Cham, 162-169, https://doi.org/10.1007/978-3-030-27544-0_13, 2019.

Foggia, P., Saggese, A., and Vento, M.: Real-Time Fire Detection for Video-Surveillance Applications Using a Combination of Experts Based on Color, Shape, and Motion, IEEE Transactions on Circuits and Systems for Video Technology, 25, 1545-1556, https://doi.org/10.1109/TCSVT.2015.2392531, 2015.

Friedl, M., and Sulla-Menashe, D.: MCD12Q1 MODIS/Terra+Aqua Land Cover Type Yearly L3 Global 500m SIN Grid V006 [Data set], https://doi.org/10.5067/MODIS/MCD12Q1.006, 2020.

Gaur, A., Singh, A., Kumar, A., Kumar, A., and Kapoor, K.: Video Flame and Smoke Based Fire Detection Algorithms: A Literature Review, Fire Technol, 56, 1943-1980, https://doi.org/10.1007/s10694-020-00986-y, 2020.

Geetha, S., Abhishek, C. S., and Akshayanat, C. S.: Machine vision based fire detection techniques: a survey, Fire Technology, 57(2), 591-623, https://doi.org/10.1007/s10694-020-01064-z, 2021.

Geng, Y.: Fire-smoke-detect-dataset, GitHub [data set], https://github.com/gengyanlei/fire-detect-yolov4, 2020.

Gibson, R., Danaher, T., Hehir, W., and Collins, L.: A remote sensing approach to mapping fire severity in south-eastern Australia using sentinel 2 and random forest, Remote Sensing of Environment, 240, 111702, https://doi.org/10.1016/j.rse.2020.111702, 2020.

Gong, F., Li, C., Gong, W., Li, X., Yuan, X., Ma, Y., and Song, T.: A Real-Time Fire Detection Method from Video with Multifeature Fusion, Computational Intelligence and Neuroscience, 2019, e1939171, https://doi.org/10.1155/2019/1939171, 2019.

Hu, X., Ban, Y., and Nascetti, A.: Sentinel-2 MSI data for active fire detection in major fire-prone biomes: A multi-criteria approach, International Journal of Applied Earth Observation and Geoinformation, 101, 102347, https://doi.org/10.1016/j.jag.2021.102347, 2021.

Jakovcevic T., and Krstinic D: Wildfire Observers and Smoke Recognition Homepage, Center for Wildfire Research [data set], http://wildfire.fesb.hr/index.php?option=com_content&view=article&id=49&Itemid=54, 2010.

Jocher, G., Stoken, A., Borovec, J., NanoCode012, Chaurasia, A., TaoXie, Changyu, L., V, A., Laughing, tkianai, yxNONG, Hogan, A., lorenzomammana, AlexWang1900, Hajek, J., Diaconu, L., Marc, Kwon, Y., oleg, wanghaoyang0106, Defretin, Y., Lohia, A., ml5ah, Milanko, B., Fineran, B., Khromov, D., Yiwei, D., Doug, Durgesh, and Ingham, F.: ultralytics/yolov5: v5.0 - YOLOv5-P5 640 models, AWS, Supervise.ly and YouTube integrations, Zenodo [code], https://doi.org/10.5281/zenodo.4679653, 2021.

Ko, B. C., Kwak, J.-Y., and Nam, J.-Y.: Wildfire smoke detection using temporospatial features and random forest classifiers, OE, 51, 017208, https://doi.org/10.1117/1.OE.51.1.017208, 2012.

Lahtinen, T., Turtiainen, H., and Costin, A.: Brima: Low-Overhead Browser-Only Image Annotation Tool (Preprint), in:
490   2021 IEEE International Conference on Image Processing (ICIP), 2021 IEEE International Conference on Image Processing (ICIP), 2633-2637, https://doi.org/10.1109/ICIP42928.2021.9506683, 2021.

Li, X., Wang, W., Wu, L., Chen, S., Hu, X., Li, J., Tang, J., and Yang, J.: Generalized Focal Loss: Learning Qualified and Distributed Bounding Boxes for Dense Object Detection, in: Advances in Neural Information Processing Systems, 21002-21012, 2020.

495 Lin, T.-Y., Maire, M., Belongie, S., Hays, J., Perona, P., Ramanan, D., Dollár, P., and Zitnick, C. L.: Microsoft COCO: Common Objects in Context, in: Computer Vision - ECCV 2014, Cham, 740-755, https://doi.org/10.1007/978-3-319-10602-1_48, 2014.

Liu, Z., Lin, Y., Cao, Y., Hu, H., Wei, Y., Zhang, Z., Lin, S., and Guo, B.: Swin Transformer: Hierarchical Vision Transformer Using Shifted Windows, in: Proceedings of the IEEE/CVF International Conference on Computer Vision,
500   10012-10022, 2021.

Muhammad, K., Ahmad, J., and Baik, S. W.: Early fire detection using convolutional neural networks during surveillance for effective disaster management, Neurocomputing, 288, 30-42, https://doi.org/10.1016/j.neucom.2017.04.083, 2018.

Pande, B., Padamwar, K., Bhattacharya, S., Roshan, S., and Bhamare, M.: A Review of Image Annotation Tools for Object Detection, in: 2022 International Conference on Applied Artificial Intelligence and Computing (ICAAIC), 2022
505   International Conference on Applied Artificial Intelligence and Computing (ICAAIC), 976-982, https://doi.org/10.1109/ICAAIC53929.2022.9792665, 2022.

Qin, X., He, S., Zhang, Z., Dehghan, M., and Jagersand, M.: ByLabel: A Boundary Based Semi-Automatic Image Annotation Tool, in: 2018 IEEE Winter Conference on Applications of Computer Vision (WACV), 2018 IEEE Winter Conference on Applications of Computer Vision (WACV), 1804-1813, https://doi.org/10.1109/WACV.2018.00200,
510   2018.

Redmon, J., Divvala, S., Girshick, R., and Farhadi, A.: You Only Look Once: Unified, Real-Time Object Detection, in: Proceedings of the IEEE Conference on Computer Vision and Pattern Recognition, 779-788, 2016.

Ren, S., He, K., Girshick, R., and Sun, J.: Faster R-CNN: Towards Real-Time Object Detection with Region Proposal Networks, in: Advances in Neural Information Processing Systems, 2015.

515 Shamsoshoara, A., Afghah, F., Razi, A., Zheng, L., Fulé, P. Z., and Blasch, E.: Aerial imagery pile burn detection using deep learning: The FLAME dataset, Computer Networks, 193, 108001, https://doi.org/10.1016/j.comnet.2021.108001, 2021.

Sharma, J., Granmo, O. C., Goodwin, M., and Fidje, J. T.: Deep convolutional neural networks for fire detection in images, in: International conference on engineering applications of neural networks, Springer, Cham, 183-193, 2017.

Sharma, M., Liang, F., Cota, A., Rieger, B., rahullb, marcelolpinto, Gantos, N., paultancre, hkuyam008, Quinn, R., and1can,
520   Lin, R., raphaeljafriLB, Clauss, C., and Vu, T. M.: Labelbox, Github [code], https://github.com/Labelbox, 2022.

Töreyin, B. U., Dedeoğlu, Y., and Çetin, A. E.: Wavelet based real-time smoke detection in video, in: 2005 13th European Signal Processing Conference, 2005 13th European Signal Processing Conference, 1-4, 2005.

Torralba, A., and Efros, A. A.: Unbiased look at dataset bias, in: CVPR, IEEE, 1521-1528, https://doi.org/10.1109/CVPR.2011.5995347, 2011.

525   Total Commander: https://www.ghisler.com/index.htm, last access: 15 November 2022.

Wada, K., mpitid, Buijs, M., Zhang, C. N., なるみ, Bc., Kubovčík, M., Myczko A., latentix, Zhu, L. N., Yamaguchi, Fujii, S., iamgd67, IlyaOvodov, Patel, A., Clauss, C., Kuroiwa, E., Iyengar, R., Shilin, S., Malygina, T., …Toft. H.: wkentaro/labelme: v4.6.0, Zenodo [code], https://doi.org/10.5281/zenodo.5711226, 2021.

Wang, M., Jiang, L., Yu, D., Tuo, T., Yue, P.: FASDD: An Open-access 100,000-level Flame And Smoke Detection Dataset

530   for Deep Learning in Fire Detection, Science Data Bank [data set], https://doi.org/10.57760/sciencedb.j00104.00103, 2022.

Wang, S., He, Y., Yang, H., Wang, K., and Wang, J.: Video smoke detection using shape, color and dynamic features, Journal of Intelligent & Fuzzy Systems, 33, 305-313, https://doi.org/10.3233/JIFS-161605, 2017.

Yuan, F.: Video-based smoke detection with histogram sequence of LBP and LBPV pyramids, Fire Safety Journal, 46, 132-

535   139, https://doi.org/10.1016/j.firesaf.2011.01.001, 2011.

Yue, P., Shangguan, B., Hu, L., Jiang, L., Zhang, C., Cao, Z., and Pan, Y.: Towards a training data model for artificial intelligence in earth observation, International Journal of Geographical Information Science, 1-25, https://doi.org/10.1080/13658816.2022.2087223, 2022.

Zhang, Q., Lin, G., Zhang, Y., Xu, G., and Wang, J.: Wildland Forest Fire Smoke Detection Based on Faster R-CNN using

540   Synthetic Smoke Images, Procedia Engineering, 211, 441-446, https://doi.org/10.1016/j.proeng.2017.12.034, 2018.